Spatial and temporal control of populations, branching ratios, and electronic coherences in LiH by a single one-cycle infrared pulse

Astrid Nikodem,[1] R. D. Levine,[2,3] and F. Remacle[1,2,*]

[1]*Department of Chemistry, University of Liege, B4000 Liege, Belgium*

[2]*The Fritz Haber Research Center for Molecular Dynamics and Institute of Chemistry, The Hebrew University of Jerusalem, Jerusalem 91904, Israel*

[3]*Crump Institute for Molecular Imaging and Department of Molecular and Medical Pharmacology, David Geffen School of Medicine and Department of Chemistry and Biochemistry, University of California, Los Angeles, California 90095, USA*

(Received 15 October 2016; revised manuscript received 19 February 2017; published 12 May 2017)

Dynamical computations demonstrate considerable selectivity over the fragmentation channels of the LiH molecule via the polarization and the carrier envelope phase (CEP) of a single ultrashort one-cycle strong IR pulse. For aligned molecules, control of the CEP allows building nonstationary coherent electronic wave packets of contrasting ionic character, either $Li^{\delta+}H^{\delta-}$ or $Li^{\delta-}H^{\delta+}$. The complementary coherences are maintained all the way to dissociation. The direction of the electric field at its maximum points either towards the Li or towards the H atom, which selectively steers the nuclear dynamics to specific dissociation products.

DOI: 10.1103/PhysRevA.95.053404

I. INTRODUCTION

Due to their broad bandwidths, ultrashort attopulses [1–5] excite molecules to coherent nonequilibrium electronic wave packets on a time scale shorter than the response of the nuclei. As a result, the nonequilibrium electron density is a coherent superposition of several electronic states and can beat between different parts of the molecule. For modular molecules this beating causes migration of charge between the different modules. Tailoring the electronic density in space and time via the parameters of the pulse [6], and in particular by varying the value of the carrier envelope phase (CEP) [7] for tailoring the electric field, was suggested early on as a means for controlling reactivity by steering the nuclear motion towards the desired products. This control of the asymptotic channels is possible if the selectivity of the excitation is maintained all the way to the products. In this paper, we demonstrate by quantum dynamical coupled pulse-electron-nuclei computations that the coherence imprinted by the ultrashort pulse is preserved all the way to the fragmentation for aligned LiH molecules excited by a single ultrashort one-cycle strong IR pulse.

Electron localization has been probed in diatomic cations [8–12] and larger systems [13–16] using pump-probe schemes involving atto- and femtosecond optical pulses. In these experiments the molecule is locally ionized by the pump which creates a nonstationary state in the cation. The cationic dynamics is then probed by monitoring the fragments by photoexcitation or ionization. Several experimental schemes rely on the CEP phase value of a CEP stable few-cycle pulse [17] for tailoring the electric field profile of the pump pulse and controlling electron localization and dissociation [8,18–25]. Photoinduced coherent electronic dynamics can also be probed using high-harmonic generation [13,26–28], transient absorption spectroscopy [29–31], time-resolved molecular-frame photoelectron-angular distribution [32], and attoclock measurements [33,34].

Here, we couple the nonequilibrium electronic dynamics induced by the interaction with a single, strong, ultrashort optical pulse [6,35–40] to nuclear motion including nonadiabatic coupling [8,41–52]. We show that switching the CEP value of the pump pulse from 0 to π controls the fragmentation yields of the different dissociation asymptotes. Nearly one-cycle CEP stable IR pulses can be experimentally synthesized for a wide range of IR wavelengths [18,20,53–57]. For the polar LiH molecule, changing the value of the CEP of the nearly one-cycle pulse allows selecting excited states of opposite polarities, depending on whether the electric field at its maximum points to the Li or to the H atoms [7,58]. As a result, the nonstationary electronic wave packet built at the end of the pulse has a different ionic character, either $Li^{\delta+}H^{\delta-}$ or $Li^{\delta-}H^{\delta+}$, and this steers the nuclear dynamics to different dissociation asymptotes. We further show that changing the value of the CEP by π prepares at the end of the pulse nonstationary states that are not only of complementary polarity but also of opposite coherence. We demonstrate that this coherence can be spectroscopically monitored by transient absorption that probes the phase of electronic coherences and of the charge migration.

II. NONEQUILIBRIUM ELECTRON-NUCLEI DYNAMICS

LiH is a heteronuclear diatomic molecule with a dense manifold of low-lying excited electronic states of different polarities in the UV range that fragment into chemically different species. LiH is therefore an ideal prototype for investigating charge migration and dissociation control.

LiH electronic states have been extensively studied by us [7,52,58–60] and others [61–64]. The electronic states were computed at Multi Reference Configuration Interaction (MRCI) level using the quantum chemistry code MOLPRO [65]; see the Supplemental Material (SM) [66] for details. Since we report on pulses polarized along the molecular axis, we restrict the dynamics to the Σ manifold of states. The computed potential energy curves of all the excited Σ states have shallow minima, as can be seen from Fig. 1(a). The lowest excited

*fremacle@ulg.ac.be

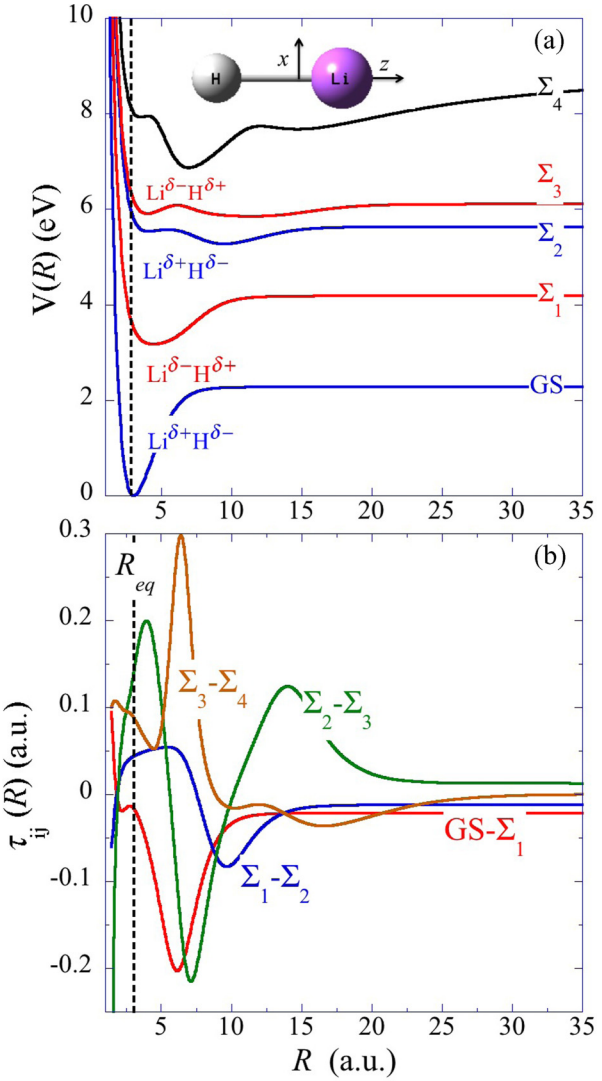

FIG. 1. (a) Potential energy curves (in eV) of the sequence of five consecutive Σ states of LiH computed at the MRCI level as a function of the internuclear distance R, in a.u. The alternating polarity of the electronic states in the Franck-Condon region is indicated. (b) NAC curves, $\tau_{ij}(R)$, in the Σ manifold. The computed value of R_{eq} (3.08 a.u., 1.63 Å) is marked by a dashed line. See SM [66] for details on the quantum chemistry computations.

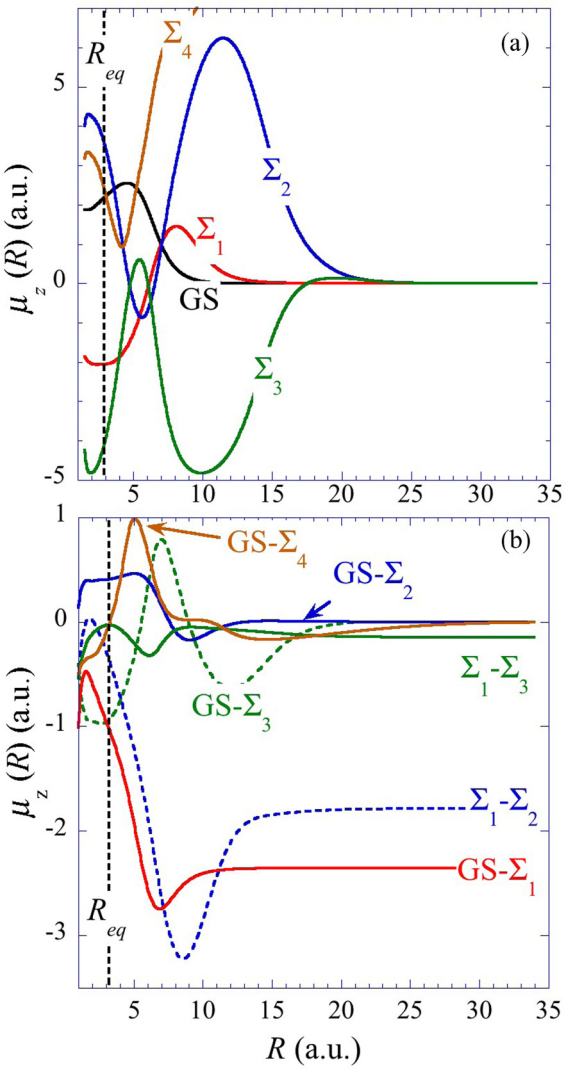

FIG. 2. (a) Permanent dipole curves of the five states of the manifold; (b) transition dipole curves for selected pairs of states. The value of the equilibrium distance in the ground state, R_{eq}, is indicated by a dashed line.

Σ and Π states are about 3.5–4 eV above the ground state (GS), and can be accessed by strong IR or UV pulses. The ground state and sequence of lowest excited Σ states exhibit alternating polarities. An excess of negative charge is localized on the H atom in the GS and in the second excited Σ state, Σ_2, which have a chemical structure $Li^{\delta+}H^{\delta-}$. In contrast, the first excited state, Σ_1, and the third one, Σ_3, are of opposite polarity, $Li^{\delta-}H^{\delta+}$. The different Σ excited states dissociate to different asymptotes. The H atom is in its GS, H(1s), and the Li atom in different excited states: Li(2s) for the GS and Li(2p), Li(3s), and Li(3p) for Σ_1, Σ_2, and Σ_3, respectively. The fourth excited state, Σ_4, dissociates to ionic products, $Li^+ + H^-$. The alternating polarity of the sequence of states implies that the Stark shifts of their potentials will be in opposite directions and this is a key to the understanding of the control and the selectivity that we report. Such a control cannot be obtained in the perturbative, one-photon limit. Opposite Stark shifts of the potential energy curves of electronic states of different polarities, as well as multiphoton processes, are essential. This mechanism is different from the one reported in [23,24] that involves inelastic recollisions of the outgoing electron with the cation.

The nonadiabatic couplings (NACs), $\tau_{ij}(R)$, between the different adiabatic states are plotted in Fig. 1(b) for selected pairs of Σ states, i and j. Only the pair of Σ_2 and Σ_3 states, which are close in energy for the whole range of internuclear distances, is significantly affected by nonadiabatic coupling. Other NAC matrix elements are more localized at smaller internuclear distances.

The computed permanent dipole curves and transition dipole moments along the bond direction are plotted in Figs. 2(a) and 2(b), respectively. About the equilibrium position ($R_{eq} = 3.08$ a.u.), the transition dipoles reflect the

polarity of the different Σ states. The equilibrium dipole moment of the GS is large enough [+2.24 a.u.; see Fig. 2(a)] that LiH could be spatially oriented experimentally [67–69]. The molecular-frame orientation is shown as an inset in Fig. 1(a) where the bond is along the z axis with the Li atom in the $+z$ direction.

Using pump pulses of different polarizations with respect to the molecular axis one can create nonstationary electronic densities that rotate perpendicular or parallel to the LiH bond [70]. In this study we report on the dynamics induced by pump pulses polarized along the molecular axis. As a hydride LiH has a rather long rotational period so we take the molecule to be nonrotating. The quantum nuclear dynamics computations were carried out by solving the time-dependent Schrödinger equation (TDSE) on a grid for the nuclear motion [71–74]. The states coupled are the manifold of the five lowest bound Σ states plotted in Fig. 1(a) and do not include the high Rydberg states that converge to the continuum (Ionization Potential is 7.8 eV). The nuclear Hamiltonian includes the coupling of the molecule to the time-dependent electric field of the pump and the probe pulses in the dipole approximation and the nonadiabatic coupling (NAC) between the Σ states. Since the pulse is an essentially one-cycle IR pulse that photoexcites the low-lying Σ states, the probability that the molecule photoionizes through a multiphoton process during the pulse is low and is not included in the dynamical simulations. The matrix form of the Hamiltonian on the grid in the basis of the adiabatic electronic states is given by

$$\begin{aligned} H_{ig,jg'}(t) = & \left(-\frac{\hbar^2}{2\mu}\nabla_R^2\right)_{g,g}\delta_{ij} + V_{ig,jg'}\delta_{ij}\delta_{gg'} \\ & -\mathbf{E}(t)\left(\boldsymbol{\mu}^{elec}_{ig,jg'} + \boldsymbol{\mu}^{nucl}_{gg'}\delta_{ij}\right)\delta_{gg'}. \\ & -\frac{\hbar^2}{2\mu}\Bigg[2\tau_{ig,jg}(\nabla_R)_{gg'} + \sum_l \tau_{ig,lg'}\tau_{lg',jg}\delta_{gg'} \\ & +g_{ig,jg'}\delta_{gg'}\Bigg]. \end{aligned} \tag{1}$$

In Eq. (1), i and j are the index of the adiabatic electronic states and g and g' are indices of grid points. μ is the reduced mass of LiH, $V_i(R)$'s are the potential energy curves plotted in Fig. 1(a), and $\boldsymbol{\mu}(R) = \boldsymbol{\mu}^{elec}(R) + \boldsymbol{\mu}^{nucl}(R)$ is the total molecular dipole moment vector; see Eq. (2) below. $\mathbf{E}(t)$ is the electric field vector of the pump and the probe pulses and the last terms in Eq. (1) are the nonadiabatic coupling matrix elements with $\tau_{ij} = \langle\psi_i(r;R)|\nabla_R|\Psi_j(r;R)\rangle$ [see Fig. 1(b)] and $g_{ij}(R) = \nabla_R[\tau_{ij}(R)]$.

In the grid representation for the nuclear coordinate R, all the operators in Eq. (1) are local except the nuclear kinetic energy and the nuclear-momentum-dependent term of the nonadiabatic coupling terms, $\tau_{ij}(R)$. We define the Gaussian electric field time profile, $\mathbf{E}_p(t)$, of each pulse from the vector potential, $\mathbf{A}_p(t)$, $d\mathbf{E}_p(t)/dt = (-1/c)\partial\mathbf{A}_p(t)/\partial t$, with $\mathbf{A}_p = \frac{-\mathbf{E}_p c}{\omega_p} f(t)\sin(\omega_p t + \phi_p)$ where ϕ_p is the CEP, c the speed of light, and ω_p the carrier frequency. This ensures that there is no dc or low-frequency component in the Fourier transform of $\mathbf{E}(t)$. The vector potential, $\mathbf{A}_p(t)$, for each pulse, p, has a Gaussian envelope, $f(t) = \exp[(t-t_p)^2/{\sigma_p}^2]$ centered at the time t_p. The polarization of the pulse is along the bond axis, $\mathbf{E}_p = |E_z^p|\mathbf{e}_z$. The amplitudes $c_{ig}(t)$ of the wave function in the electronic state i at the grid point g, $\Psi(t) = \sum_{i,g} c_{ig}(t)|i\rangle$, are computed by numerically integrating the TDSE, $i\hbar dc_{ig}(t)/dt = \sum_{jg'} H_{ig,jg'}(t)c_{jg'}(t)$, for the Hamiltonian of Eq. (1).

III. SELECTIVE FRAGMENTATION BY A SINGLE CEP CONTROLLED ONE-CYCLE IR PULSE

The pump is a CEP controlled essentially one-cycle pulse polarized along the molecular axis with a carrier frequency, ω_p, of 1.55 eV (800 nm). The pulse we use is strong (5.61×10^{13} W/cm^2, $|E_z^p| = 0.04$ a.u.) and its envelope is short ($\sigma = 0.68$ fs, FWHM = 1.13 fs) so as to span a single large maximum, which is necessary for the selectivity mechanism discussed here. There are also inevitably two secondary small maxima because we impose that the area of $\mathbf{E}(t)$ is equal to zero, so as not to have a component at zero frequency. There are 1.5 oscillations of the electric field within the short pulse envelope, oscillations that are faster than the period of the carrier wave (800 nm corresponds to a period of 2.66 fs). This is reflected in the Fourier transform of the pulse given in Fig. S1 [66], which is an asymmetric broad peak with a maximum at 2.27 eV. The essential feature of the pulse for the control mechanism by the value of the CEP is that it is strong, so that multiphoton excitation is allowed and that the envelope is such that the electric field exhibits a main maximum significantly higher than the secondary ones. A CEP ϕ_p equal to 0 corresponds to a maximum of the electric field in the $+z$ direction, pointing to the Li atom, while $\phi_p = \pi$ corresponds to a maximum of the electric field pointing to the H atom, in the $-z$ direction. We start the dynamical simulation from the ground vibrational state of the ground electronic state. The populations, $p_i(t) = \sum_g |c_{ig}(t)|^2$, in the different excited Σ states are plotted in Fig. 3(a) for the pulse with a CEP $\phi_p = 0$ and Fig. 3(b) for that with $\phi_p = \pi$. The two panels of Fig. 3 show that changing only the value of the CEP of an essentially one-cycle pulse leads to very different nonequilibrium electronic densities, as reflected in the different values of the populations in the Σ manifold at the end of the pulse. For the strong pulses used in Fig. 3, different values of the phase, ϕ_p, lead to different populations in the excited states. Pumping with a CEP = 0 one-cycle pulse, Fig. 3(a), the highest population is in Σ_2 while for the CEP = π pump pulse, the highest population is in Σ_1 and Σ_3. The selectivity of the excitation can be qualitatively understood on the basis of the sign of Stark shift in the energies of the excited electronic states which will be opposite for states of different polarities. Excited states with a permanent dipole antiparallel to that of the GS, a dipole pointing to the H atom in the Franck-Condon region, such as Σ_1 and Σ_3, are preferentially accessed by the CEP = π pulse, while Σ_2, which is of opposite polarity, is preferentially populated by the CEP = 0 pulse. Changing the value of the CEP controls the fragmentation yields of the two states that dissociate along Σ_2 and Σ_3. Changing the CEP by π inverts the yield ratio between the two states. A value of the CEP = 0 leads to a branching ratio of $Y_{\Sigma_2}/Y_{\Sigma_3} = 2.45$ while the pulse with a CEP = π leads to a branching ratio $Y_{\Sigma_2}/Y_{\Sigma_3} = 0.29$. The rates for these direct

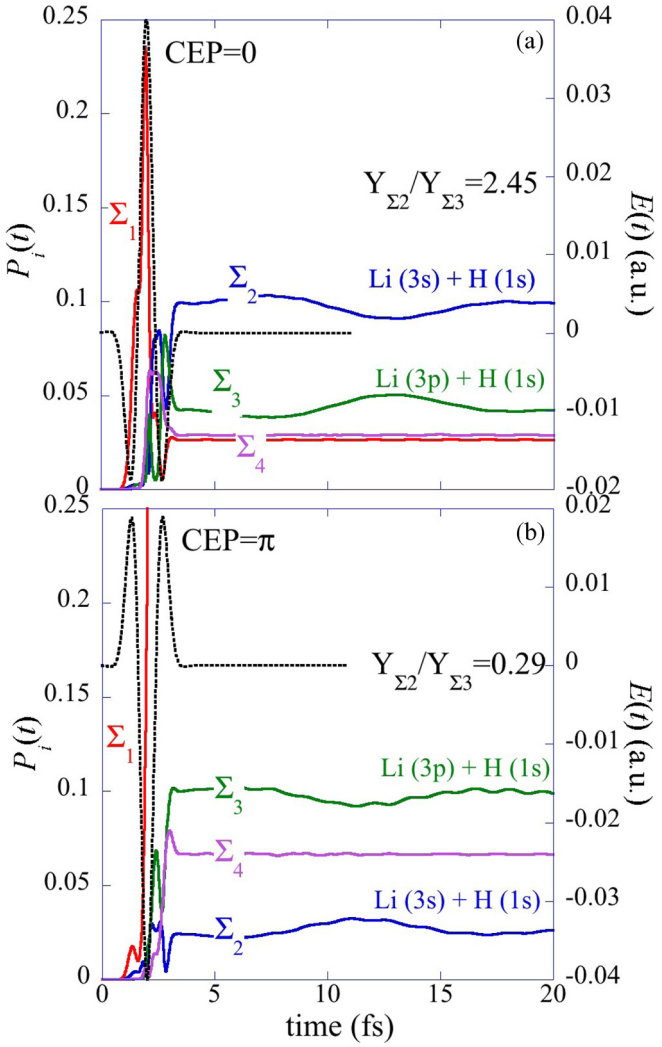

FIG. 3. Effect of the CEP ϕ_p on the populations of the different electronic states, $p_i(t)$, in the Σ manifold. (a) CEP = 0. The highest population is in the Σ_2 state, asymptotically 9.72% with 4.40% in Σ_3. (b) CEP = π; the maximum of population is in Σ_1 (48.7%, not shown) and the branching ratio of the populations in Σ_2 and Σ_3 is opposite (asymptotically 2.65% in Σ_2 and 9.82% in Σ_3). The Σ_1 state does not dissociate for these excitation pulses. The small population in Σ_4 is about equal for either value of the CEP. The profile of the electric field of the pump pulse is shown by a dotted line (scale on the right y axis). The small exchange of populations between the Σ_2 and Σ_3 states is due to their nonadiabatic coupling. By about 20 fs the molecule is in the asymptotic range so that the dissociation is very direct.

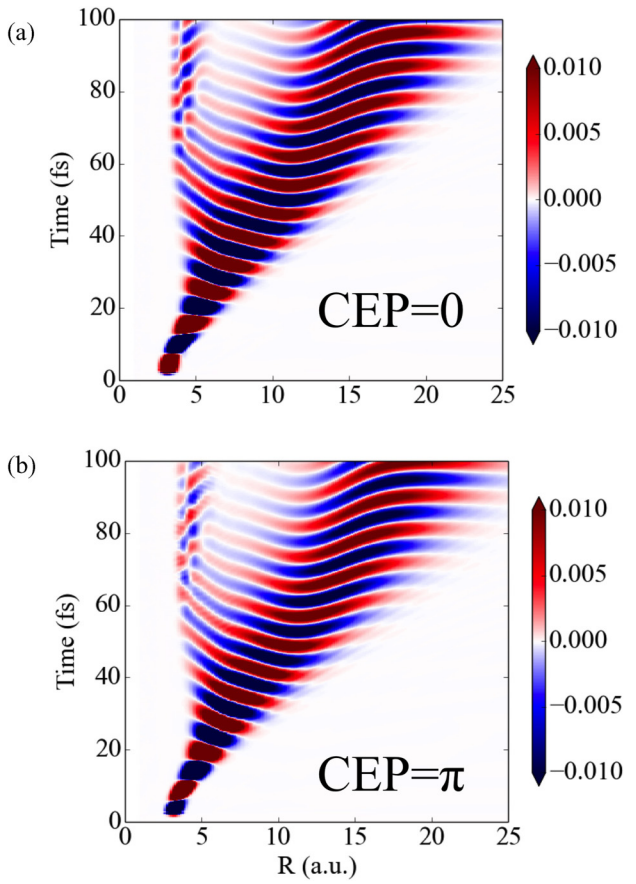

FIG. 4. Heat maps of the real part of the electronic coherence, $\mathrm{Re}[\rho_{\Sigma_2-\Sigma_3}(R_g,t)]$, between the states Σ_2 and Σ_3. Plotted as a function of the Li-H distance R (x axis) and of time (y axis), for a pulse with a CEP = 0 (upper panel) and π (lower panel), with the same parameters as in Fig. 3.

dissociations are in the picosecond range, 0.01 fs^{-1} for Σ_2 and 0.006 fs^{-1} for Σ_3.

As can be seen from Fig. S2 [66]—which reports the R dependence of the coefficients, $c_{\Sigma_2 g}(t)$ and $c_{\Sigma_3 g}(t)$, computed at the end of the pulse ($t = 4$ fs) for the two values of the CEP—the value of the CEP is imprinted in the coefficients of the wave packet. The CEP = 0 pulse prepares a state that we approximate as $|\Psi_{\mathrm{CEP}=0}(R_g,t = 4\mathrm{fs})\rangle = a_{Rg}(t = 4\mathrm{fs})|\Sigma_2(R_g)\rangle + b_{Rg}(t = 4\mathrm{fs})|\Sigma_3(R_g)\rangle$ at the end of the pulse. In the state prepared by the CEP = π pulse, the absolute values of the amplitudes on the two electronic states are almost switched because of the polarity control and there is a phase shift of about π, $|\Psi_{\mathrm{CEP}=\pi}(R_g,t = 4\,\mathrm{fs})\rangle \approx b_{Rg}(t = 4\,\mathrm{fs})|\Sigma_2(R_g)\rangle - a_{Rg}(t = 4\,\mathrm{fs})|\Sigma_3(R_g)\rangle$. The electronic coherence between the states Σ_2 and Σ_3 at a given value R_g on the grid is given by $\rho_{\Sigma_2-\Sigma_3}(R_g,t) = c^*_{\Sigma_2 g}(t)c_{\Sigma_3 g}(t)$. Using the simplified forms above for the wave function, we get $\rho^{\mathrm{CEP}=0}_{\Sigma_2-\Sigma_3}(R_g,t) = a^*_g(t)b_g(t)$ for the CEP = 0 pulse, while for the CEP = π pulse, the sign is opposite $\rho^{\mathrm{CEP}=\pi}_{\Sigma_2-\Sigma_3}(R_g,t) \approx -a_g(t)b^*_g(t)$. The two coherences beat with a frequency given by the energy difference, $\Delta E_{\Sigma_2-\Sigma_3}(R) = V_{\Sigma_3}(R) - V_{\Sigma_2}(R) \approx 0.5$ eV (period = 8.2 fs) between the field free state electronic energies and they have opposite sign for their real parts. We show in Fig. 4 heat maps of the real part of the $\rho_{\Sigma_2-\Sigma_3}(R_g,t)$ as a function of time (ordinate) and of its localization in R (abscissa), computed for electron-nuclei dynamics induced by the two pulses of opposite CEP shown in Fig. 3. Figure 4 shows that the difference in the phase of the electronic coherence prepared by the two pulses is preserved in the presence of nuclear motion both in the part of the wave packet that remains bound and in the part that dissociates all the way to the dissociation asymptote. The heat maps of the imaginary parts are shown in Fig. S3 [66].

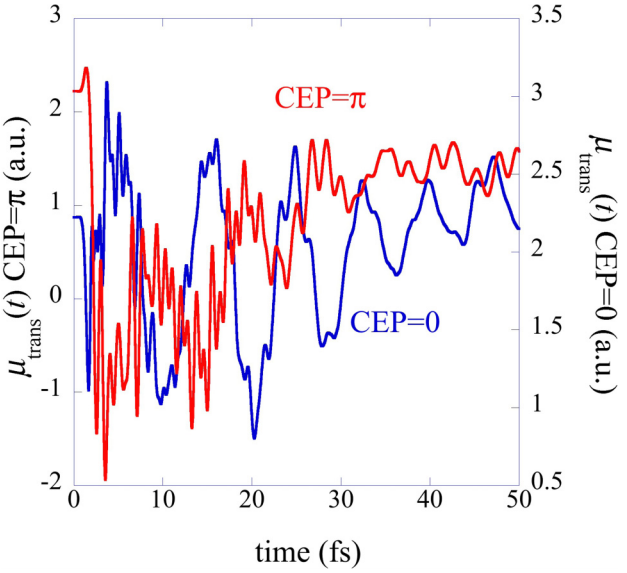

FIG. 5. Computed transition dipole, $\mu_{\text{trans}}(t)$, for the two pulses. Note that the oscillations with a period ≈8 fs, which correspond to the $\Sigma_2-\Sigma_3$ coherence, have opposite phase for the two pump pulses.

The difference in the wave functions prepared by the two pulses explains why in Fig. 3, the small oscillations in the populations of Σ_2 and Σ_3 that are due to the nonadiabatic coupling have opposite phases.

IV. PROBING OF THE ELECTRONIC COHERENCE

The nonstationary character of the coherent state prepared by the pulse means that the LiH molecule will have a time-dependent dipole, $\mu(t)$ [51,52], which includes both nuclear and electronic contributions:

$$\begin{aligned}\boldsymbol{\mu}_{tot}(t) &= \sum_g \rho(R_g,t)\boldsymbol{\mu}_{tot}(R_g)\\ &= \sum_{ig,jg} c^*_{ig}(t)c_{jg}(t)\mu^{ele}_{i,j}(R_g)\\ &\quad + \sum_{ig} |c_{ig}(t)|^2\boldsymbol{\mu}^{nucl}(R_g)\\ &= \sum_{ig} \left|c_{ig}(t)\right|^2\left[\boldsymbol{\mu}^{elec}_{ii}(R_g)+\boldsymbol{\mu}^{nucl}(R_g)\right]\\ &\quad + \sum_g 2\mathrm{Re}\left(\sum_{i>j} c^*_{ig}(t)c_{jg}(t)\boldsymbol{\mu}^{ele}_{i,j}(R_g)\right), \qquad (2)\end{aligned}$$

and which has both a diagonal and a coherent, transition dipole, contribution. Figure 5 shows the time-dependent transition dipole component, that is, the part of the dipole that is nondiagonal in the electronic states, $\mu_{\text{trans}}(t) = \sum_g 2\mathrm{Re}(\sum_{i>j} c^*_{ig}(t)c_{jg}(t)\boldsymbol{\mu}^{ele}_{i,j}(R_g))$, computed for the two pulses of opposite CEP used in Fig. 3. $\mu_{\text{trans}}(t)$ clearly exhibits oscillations with a period of ≈8 fs, which corresponds to the period of the $\Sigma_2 - \Sigma_3$ coherence. Moreover these oscillations have opposite phase for the two pump pulses, which reflects the π difference in the values of their CEP. In addition, the rapid oscillations of $\mu_{\text{trans}}(t)$, of the order of 1 fs, reflect the transition frequencies between the excited states and the GS. The slower modulation is due to nuclear motion in the bound electronic states. The vibrational period of the GS is 20 fs and that of the first excited state Σ_1 is equal to 80 fs [52].

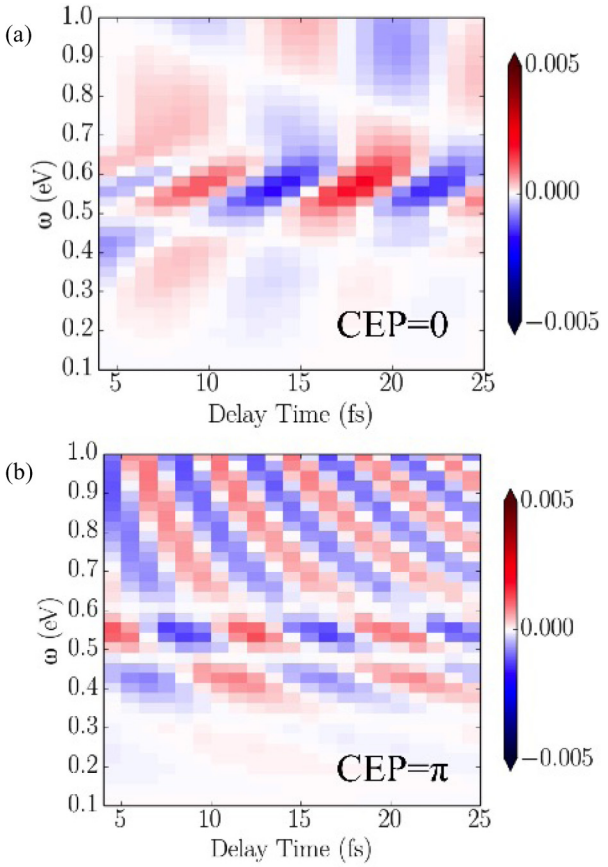

FIG. 6. Heat maps of the response $S(\omega)$ computed for the pump pulse with a CEP = 0 (top) and with a CEP = π (bottom) for a range of delay times between the pump and the probe of 20 fs (x axis). The y axis is centered on the frequency range of the Σ_2-Σ_3 electronic coherence.

The nonstationary electronic polarization, a signature of the excitation of a coherent state, can be probed by a second pulse [31]. We computed the linear response function, $S(\omega)$, of the time-dependent dipole prepared by the pump pulse as in Refs. [31,75,76], $S(\omega) = -2\mathrm{Im}[\boldsymbol{\mu}(\omega)\mathbf{E}^*(\omega)]$. $\boldsymbol{\mu}(\omega)$ and $\mathbf{E}(\omega)$ are the Fourier transform (FT) of the dipole, $\boldsymbol{\mu}(t)$, Eq. (2), and of the complete time course of the electric field, $\mathbf{E}(t)$, including the pump and the probe pulses. The probe is a one-cycle IR pulse with the same parameters as the CEP = 0 pulse used for the pump, but a far lower strength, $|E^p_z| = 0.001$ a.u. Figure 6 shows heat maps of the response, $S(\omega)$, computed for the two pump pulses, top with a CEP = 0 and bottom with a CEP = π. The heat maps are plotted as a function of the delay time between the pump and the probe (abscissa) and as a function of the frequency ω (ordinate). The frequency axis is centered on the transition frequency, $\Delta E_{\Sigma_2-\Sigma_3} \simeq 0.5$ eV. Absorption corresponds to a positive value of $S(\omega)$ and is plotted in blue; emission which corresponds to a negative value is plotted in red. The delay time range starts just after the end of the pump

pulse at 4 fs, up to 25 fs. Comparing the two heat maps shows that the response function $S(\omega)$ provides a suitable probe for the electronic coherence and its phase. Figure 6 shows that the response function oscillates as a function of the delay time with the period of ≈8 fs that corresponds to the period of the electronic coherence between Σ_2 and Σ_3. Moreover the response oscillations are of opposite phase depending of the value of the CEP of the pump pulse and reflect the π phase difference in the real part of the electronic coherence created at the end of the pulse. The value of the CEP phase is also reflected in the heat maps of the response centered at Σ_1-Σ_2 and Σ_1-Σ_3 transition frequencies, at ≈2.5 eV, plotted in Fig. S4 [66]. In Fig. S4, in addition to the fast beating of ≈1.6 fs, which corresponds to the Σ_1-Σ_2 and Σ_1-Σ_3 transitions, one also distinguishes a clear modulation due to the Σ_2-Σ_3 coherence, with a period of ≈8 fs.

V. CONCLUDING REMARKS

We demonstrated a switching the polarity of the nonequilibrium charge density in a modular molecule by altering the CEP of a one-cycle laser pump pulse. Controlling the polarity allows choosing alternative dissociation channels by selectively accessing different electronic excited states. Switching the polarity with the carrier phase also induces a switch of the coherence of the excited electronic wave packet. Controlling the coherence selects contrasting directions for the nonstationary charge migration, along the bond or in an opposite direction as can be probed by a second laser pulse. Controlling the coherence is also essential in quantum memory and quantum computing applications.

ACKNOWLEDGMENTS

This work is supported by the U.S. Department of Energy (DOE), Office of Science, Basic Energy Sciences (BES) under Award No. DE-SC0012628 and by the Fonds de la Recherche Fondamentale Collective (Grants No. T.0132.16 and No. 2.4545.12). We benefited from our participation in the COST (European Cooperation in Science and Technology), Grant No. CM1204, XUV/Xray light and fast ions on ultrafast chemistry (XLIC). F.R. acknowledges support from the Fonds National de la Recherche (F.R.S-F.N.R.S), Belgium.

[1] P. B. Corkum and F. Krausz, Attosecond science, Nat. Phys. **3**, 381 (2007).
[2] M. F. Kling, and M. J. J. Vrakking, Attosecond electron dynamics, Ann. Rev. Phys. Chem. **59**, 463 (2008).
[3] F. Krausz and M. Ivanov, Attosecond physics, Rev. Mod. Phys. **81**, 163 (2009).
[4] F. Lépine, G. Sansone, and M. J. J. Vrakking, Molecular applications of attosecond laser pulses, Chem. Phys. Lett. **578**, 1 (2013).
[5] F. Calegari, G. Sansone, S. Stagira, C. Vozzi, and M. Nisoli, Advances in attosecond science, J. Phys. B **49**, 062001 (2016).
[6] F. Remacle and R. D. Levine, An electronic time scale for chemistry, Proc. Natl. Acad. Sci. USA **103**, 6793 (2006).
[7] F. Remacle, M. Nest, and R. D. Levine, Laser Steered Ultrafast Quantum Dynamics of Electrons in LiH, Phys. Rev. Lett. **99**, 183902 (2007).
[8] M. F. Kling, C. Siedschlag, A. J. Verhoef, J. I. Khan, M. Schultze, T. Uphues, Y. Ni, M. Uiberacker, M. Drescher, F. Krausz, and M. J. J. Vrakking, Control of electron localization in molecular dissociation, Science **312**, 246 (2006).
[9] G. Sansone, F. Kelkensberg, J. F. Perez-Torres, F. Morales, M. F. Kling, W. Siu, O. Ghafur, P. Johnsson, M. Swoboda, E. Benedetti, F. Ferrari, F. Lepine, J. L. Sanz-Vicario, S. Zherebtsov, I. Znakovskaya, A. L'Huillier, M. Y. Ivanov, M. Nisoli, F. Martin, and M. J. J. Vrakking, Electron localization following attosecond molecular photoionization, Nature **465**, 763 (2010).
[10] S. Haessler, J. Caillat, W. Boutu, C. Giovanetti-Teixeira, T. Ruchon, T. Auguste, Z. Diveki, P. Breger, A. Maquet, B. Carre, R. Taieb, and P. Salieres, Attosecond imaging of molecular electronic wavepackets, Nat. Phys. **6**, 200 (2010).
[11] W. Li, A. A. Jaron-Becker, C. W. Hogle, V. Sharma, X. Zhou, A. Becker, H. C. Kapteyn, and M. M. Murnane, Visualizing electron rearrangement in space and time during the transition from a molecule to atoms, Proc. Natl. Acad. Sci. USA **107**, 20219 (2010).
[12] P. Ranitovic, C. W. Hogle, P. Rivière, A. Palacios, X. M. Tong, N. Toshima, A. González-Castrillo, L. Martin, F. Martín, M. M. Murnane, and H. Kapteyn, Attosecond vacuum UV coherent control of molecular dynamics, Proc. Natl. Acad. Sci. USA **111**, 912 (2014).
[13] X. Zhou, P. Ranitovic, C. W. Hogle, J. H. D. Eland, H. C. Kapteyn, and M. M. Murnane, Probing and controlling non-Born-Oppenheimer dynamics in highly excited molecular ions, Nat. Phys. **8**, 232 (2012).
[14] C. Neidel, J. Klei, C. H. Yang, A. Rouzée, M. J. J. Vrakking, K. Klünder, M. Miranda, C. L. Arnold, T. Fordell, A. L'Huillier, M. Gisselbrecht, P. Johnsson, M. P. Dinh, E. Suraud, P. G. Reinhard, V. Despré, M. A. L. Marques, and F. Lépine, Probing Time-Dependent Molecular Dipoles on the Attosecond Time Scale, Phys. Rev. Lett. **111**, 033001 (2013).
[15] L. Belshaw, F. Calegari, M. J. Duffy, A. Trabattoni, L. Poletto, M. Nisoli, and J. B. Greenwood, Observation of ultrafast charge migration in an amino acid, J. Phys. Chem. Lett. **3**, 3751 (2012).
[16] F. Calegari, D. Ayuso, A. Trabattoni, L. Belshaw, S. De Camillis, S. Anumula, F. Frassetto, L. Poletto, A. Palacios, P. Decleva, J. B. Greenwood, F. Martín, and M. Nisoli, Ultrafast electron dynamics in phenylalanine initiated by attosecond pulses, Science **346**, 336 (2014).
[17] M. F. Kling, P. von den Hoff, I. Znakovskaya, and R. de Vivie-Riedle, (Sub-)femtosecond control of molecular reactions via tailoring the electric field of light, Phys. Chem. Chem. Phys. **15**, 9448 (2013).
[18] E. Goulielmakis, M. Schultze, M. Hofstetter, V. S. Yakovlev, J. Gagnon, M. Uiberacker, A. L. Aquila, E. M. Gullikson, D. T. Attwood, R. Kienberger, F. Krausz, and U. Kleineberg, Single-cycle nonlinear optics, Science **320**, 1614 (2008).

[19] M. Kübel, R. Siemering, C. Burger, N. G. Kling, H. Li, A. S. Alnaser, B. Bergues, S. Zherebtsov, A. M. Azzeer, I. Ben-Itzhak, R. Moshammer, R. de Vivie-Riedle, and M. F. Kling, Steering Proton Migration in Hydrocarbons Using Intense Few-Cycle Laser Fields, Phys. Rev. Lett. **116**, 193001 (2016).

[20] G. G. Paulus, F. Grasbon, H. Walther, P. Villoresi, M. Nisoli, S. Stagira, E. Priori, and S. De Silvestri, Absolute-phase phenomena in photoionization with few-cycle laser pulses, Nature **414**, 182 (2001).

[21] H. Li, B. Mignolet, G. Wachter, S. Skruszewicz, S. Zherebtsov, F. Süßmann, A. Kessel, S. A. Trushin, N. G. Kling, M. Kübel, B. Ahn, D. Kim, I. Ben-Itzhak, C. L. Cocke, T. Fennel, J. Tiggesbäumker, K. H. Meiwes-Broer, C. Lemell, J. Burgdörfer, R. D. Levine *et al.*, Coherent Electronic Wave Packet Motion in C60 Controlled by the Waveform and Polarization of Few-Cycle Laser Fields, Phys. Rev. Lett. **114**, 123004 (2015).

[22] S. Miura, T. Ando, K. Ootaka, A. Iwasaki, H. Xu, T. Okino, K. Yamanouchi, D. Hoff, T. Rathje, G. G. Paulus, M. Kitzler, A. Baltuška, G. Sansone, and M. Nisoli, Carrier-envelope-phase dependence of asymmetric CD bond breaking in C2D2 in an intense few-cycle laser field, Chem. Phys. Lett. **595–596**, 61 (2014).

[23] X. Xie, K. Doblhoff-Dier, S. Roither, M. S. Schöffler, D. Kartashov, H. Xu, T. Rathje, G. G. Paulus, A. Baltuška, S. Gräfe, and M. Kitzler, Attosecond-Recollision-Controlled Selective Fragmentation of Polyatomic Molecules, Phys. Rev. Lett. **109**, 243001 (2012).

[24] G. Cerullo and C. Vozzi, Viewpoint: coherent control of chemical reactions on the attosecond time scale, Physics **5**, 138 (2012).

[25] N. G. Kling, K. J. Betsch, M. Zohrabi, S. Zeng, F. Anis, U. Ablikim, B. Jochim, Z. Wang, M. Kübel, M. F. Kling, K. D. Carnes, B. D. Esry, and I. Ben-Itzhak, Carrier-Envelope Phase Control over Pathway Interference in Strong-Field Dissociation of H2+, Phys. Rev. Lett. **111**, 163004 (2013).

[26] O. Smirnova, Y. Mairesse, S. Patchkovskii, N. Dudovich, D. Villeneuve, P. Corkum, and M. Y. Ivanov, High harmonic interferometry of multi-electron dynamics in molecules, Nature **460**, 972 (2009).

[27] Y. Mairesse, J. Higuet, N. Dudovich, D. Shafir, B. Fabre, E. Mével, E. Constant, S. Patchkovskii, Z. Walters, M. Y. Ivanov, and O. Smirnova, High Harmonic Spectroscopy of Multichannel Dynamics in Strong-Field Ionization, Phys. Rev. Lett. **104**, 213601 (2010).

[28] P. M. Kraus, B. Mignolet, D. Baykusheva, A. Rupenyan, L. Horný, E. F. Penka, G. Grassi, O. I. Tolstikhin, J. Schneider, F. Jensen, L. B. Madsen, A. D. Bandrauk, F. Remacle, and H. J. Wörner, Measurement and laser control of attosecond charge migration in ionized iodoacetylene, Science **350**, 790 (2015).

[29] E. Goulielmakis, Z. H. Loh, A. Wirth, R. Santra, N. Rohringer, V. S. Yakovlev, S. Zherebtsov, T. Pfeifer, A. M. Azzeer, M. F. Kling, S. R. Leone, and F. Krausz, Real-time observation of valence electron motion, Nature **466**, 739 (2010).

[30] M. Holler, F. Schapper, L. Gallmann, and U. Keller, Attosecond Electron Wave-Packet Interference Observed by Transient Absorption, Phys. Rev. Lett. **106**, 123601 (2011).

[31] K. Ramasesha, S. R. Leone, and D. M. Neumark, Real-time probing of electron dynamics using attosecond time-resolved spectroscopy, Annu. Rev. Phys. Chem. **67**, 41 (2016).

[32] P. Hockett, C. Z. Bisgaard, O. J. Clarkin, and A. Stolow, Time-resolved imaging of purely valence-electron dynamics during a chemical reaction, Nat. Phys. **7**, 612 (2011).

[33] A. N. Pfeiffer, C. Cirelli, M. Smolarski, and U. Keller, Recent attoclock measurements of strong field ionization, Chem. Phys. **414**, 84 (2013).

[34] P. Eckle, A. N. Pfeiffer, C. Cirelli, A. Staudte, R. Dörner, H. G. Muller, M. Büttiker, and U. Keller, Attosecond ionization and tunneling delay time measurements in helium, Science **322**, 1525 (2008).

[35] H. Hennig, J. Breidbach, and L. S. Cederbaum, Electron correlation as the driving force for charge transfer: Charge migration following ionization in N-methyl acetamide, J. Phys. Chem. A **109**, 409 (2005).

[36] A. I. Kuleff and L. S. Cederbaum, Charge migration in different conformers of glycine: the role of nuclear geometry, Chem. Phys. **338**, 320 (2007).

[37] A. I. Kuleff, S. Lünnemann, and L. S. Cederbaum, Electron-correlation-driven charge migration in oligopeptides, Chem. Phys. **414**, 100 (2013).

[38] I. Barth and J. Manz, Electric ring currents in atomic orbitals and magnetic fields induced by short intense circularly polarized π laser pulses, Phys. Rev. A **75**, 012510 (2007).

[39] G. Hermann, C. Liu, J. Manz, B. Paulus, J. F. Pérez-Torres, V. Pohl, and J. C. Tremblay, Multidirectional angular electronic flux during adiabatic attosecond charge migration in excited benzene, J. Phys. Chem. A **120**, 5360 (2016).

[40] V. Despré, A. Marciniak, V. Loriot, M. C. E. Galbraith, A. Rouzée, M. J. J. Vrakking, F. Lépine, and A. I. Kuleff, Attosecond hole migration in benzene molecules surviving nuclear motion, J. Phys. Chem. Lett. **6**, 426 (2015).

[41] A. D. Bandrauk, S. Chelkowski, P. B. Corkum, J. Manz, and G. L. Yudin, Attosecond photoionization of a coherent superposition of bound and dissociative molecular states: Effect of nuclear motion, J. Phys. B **42**, 134001 (2009).

[42] Y. Ide, T. Kato, and K. Yamanouchi, Non-Born–Oppenheimer molecular wave functions of H2 by extended multi-configuration time-dependent Hartree–Fock method, Chem. Phys. Lett. **595–596**, 180 (2014).

[43] K. L. Ishikawa and T. Sato, A review on ab initio approaches for multielectron dynamics, IEEE J. Sel. Top. Quantum Electron. **21**, 1 (2015).

[44] A. Palacios, A. González-Castrillo, H. Bachau, and F. Martín, Wave packet dynamics in molecular excited electronic states, J. Phys.: Conf. Ser. **488**, 012017 (2014).

[45] T. Kato and H. Kono, Time-dependent multiconfiguration theory for ultrafast electronic dynamics of molecules in an intense laser field: electron correlation and energy re-distribution among natural orbitals, Chem. Phys. **366**, 46 (2009).

[46] H. Kono, Y. Sato, N. Tanak, T. Kato, K. Nakai, S. Koseki, and Y. Fujimura, Quantum mechanical study of electronic and nuclear dynamics of molecules in intense laser fields, Chem. Phys. **304**, 203 (2004).

[47] P. v. d. Hoff, R. Siemering, M. Kowalewski, and R. d. Vivie-Riedle, Electron dynamics and its control in molecules: From diatomics to larger molecular systems, IEEE J. Sel. Top. Quantum Electron. **18**, 119 (2012).

[48] P. von den Hoff, I. Znakovskaya, M. F. Kling, and R. de Vivie-Riedle, Attosecond control of the dissociative ionization via

electron localization: a comparison between D2 and CO, Chem. Phys. **366**, 139 (2009).

[49] M. Kowalewski, K. Bennett, J. R. Rouxel, and S. Mukamel, Monitoring Nonadiabatic Electron-Nuclear Dynamics in Molecules by Attosecond Streaking of Photoelectrons, Phys. Rev. Lett. **117**, 043201 (2016).

[50] B. H. Muskatel, F. Remacle, and R. D. Levine, AttoPhotoChemistry. Probing ultrafast electron dynamics by the induced nuclear motion: the prompt and delayed predissociation of N_2, Chem. Phys. Lett. **601**, 45 (2014).

[51] J. Ajay, J. Šmydke, F. Remacle, and R. D. Levine, Probing in space and time the nuclear motion driven by nonequilibrium electronic dynamics in ultrafast pumped N2, J. Phys. Chem. A **120**, 3335 (2016).

[52] A. Nikodem, R. D. Levine, and F. Remacle, Quantum nuclear dynamics pumped and probed by ultrafast polarization controlled steering of a coherent electronic state in LiH, J. Phys. Chem. A **120**, 3343 (2016).

[53] F. Süßmann, S. Zherebtsov, J. Plenge, N. G. Johnson, M. Kübel, A. M. Sayler, V. Mondes, C. Graf, E. Rühl, G. G. Paulus, D. Schmischke, P. Swrschek, and M. F. Kling, Single-shot velocity-map imaging of attosecond light-field control at kilohertz rate, Rev. Sci. Instrum. **82**, 093109 (2011).

[54] N. G. Johnson, O. Herrwerth, A. Wirth, S. De, I. Ben-Itzhak, M. Lezius, B. Bergues, M. F. Kling, A. Senftleben, C. D. Schröter, R. Moshammer, J. Ullrich, K. J. Betsch, R. R. Jones, A. M. Sayler, T. Rathje, K. Rühle, W. Müller, and G. G. Paulus, Single-shot carrier-envelope-phase-tagged ion-momentum imaging of nonsequential double ionization of argon in intense 4-fs laser fields, Phys. Rev. A **83**, 013412 (2011).

[55] B. E. Schmidt, A. D. Shiner, P. Lassonde, J.-C. Kieffer, P. B. Corkum, D. M. Villeneuve, and F. Légaré, CEP stable 1.6 cycle laser pulses at 1.8 μm, Opt. Express **19**, 6858 (2011).

[56] T. Fuji, Y. Nomura, and H. Shirai, Generation and Characterization of Phase-Stable Sub-Single-Cycle Pulses at 3000 cm^{-1}, IEEE J. Sel. Top. Quantum Electron. **21**, 1 (2015).

[57] T. Fuji and T. Suzuki, Generation of sub-two-cycle mid-infrared pulses by four-wave mixing through filamentation in air, Opt. Lett. **32**, 3330 (2007).

[58] M. Nest, F. Remacle, and R. D. Levine, Pump and probe ultrafast electron dynamics in LiH: a computational study, New J. Phys. **10**, 025019 (2008).

[59] F. Remacle, R. Kienberger, F. Krausz, and R. D. Levine, On the feasibility of an ultrafast purely electronic reorganization in lithium hydride, Chem. Phys. **338**, 342 (2007).

[60] F. Remacle and R. D. Levine, Attosecond pumping of nonstationary electronic states of LiH: Charge shake-up and electron density distortion, Phys. Rev. A **83**, 013411 (2011).

[61] F. X. Gadea, Accurate ab initio calculations for LiH and its ions, LiH^+ and LiH^-, Theor. Chem. Acc. **116**, 566 (2006).

[62] I. S. Ulusoy and M. Nest, The multi-configuration electron-nuclear dynamics method applied to LiH, J. Chem. Phys. **136**, 054112 (2012).

[63] I. S. Ulusoy and M. Nest, Remarks on the validity of the fixed nuclei approximation in quantum electron dynamics, J. Phys. Chem. A **116**, 11107 (2012).

[64] Y. Arasaki and K. Takatsuka, Pulse-train photoelectron spectroscopy of electronic and nuclear dynamics in molecules, ChemPhysChem **14**, 1387 (2013).

[65] H.-J. Werner, P. J. Knowles, F. R. Manby, M. Schuetz, P. Celani, G. Knizia, T. Korona, R. Lindh, A. Mitrushenkov, G. Rauhut, T. B. Adler, R. D. Amos, A. Bernhardsson, A. Berning, D. L. Cooper, M. J. O. Deegan, A. J. Dobbyn, F. Eckert, E. Goll, C. Hampel *et al.*, *MOLPRO a package of ab initio programs* (2012).

[66] See Supplemental Material at http://link.aps.org/supplemental/10.1103/PhysRevA.95.053404 for more computational details and supplementary figures.

[67] O. Ghafur, A. Rouzee, A. Gijsbertsen, W. K. Siu, S. Stolte, and M. J. J. Vrakking, Impulsive orientation and alignment of quantum-state-selected NO molecules, Nat. Phys. **5**, 289 (2009).

[68] L. Holmegaard, J. H. Nielsen, I. Nevo, H. Stapelfeldt, F. Filsinger, J. Kupper, and G. Meijer, Laser-Induced Alignment and Orientation of Quantum-State-Selected Large Molecules, Phys. Rev. Lett. **102**, 023001 (2009).

[69] P. M. Kraus, A. Rupenyan, and H. J. Wörner, High-Harmonic Spectroscopy of Oriented OCS Molecules: Emission of Even and Odd Harmonics, Phys. Rev. Lett. **109**, 233903 (2012).

[70] F. Remacle and R. D. Levine, Probing ultrafast purely electronic charge migration in small peptides, Z. Phys. Chem. **221**, 647 (2007).

[71] R. Kosloff, Time-dependent quantum-mechanical methods for molecular dynamics, J. Phys. Chem. **92**, 2087 (1988).

[72] C. P. Koch and R. Kosloff, Correlation dynamics after short-pulse photoassociation, Phys. Rev. A **81**, 063426 (2010).

[73] R. Kosloff, Propagation methods for quantum molecular dynamics, Annu. Rev. Phys. Chem. **45**, 145 (1994).

[74] D. J. Tannor, *Introduction to Quantum Mechanics. A Time-Dependent Perspective* (University Science Books, Sausalito, CA, 2007).

[75] M. B. Gaarde, C. Buth, J. L. Tate, and K. J. Schafer, Transient absorption and reshaping of ultrafast XUV light by laser-dressed helium, Phys. Rev. A **83**, 013419 (2011).

[76] W. Mengxi, C. Shaohao, C. Seth, J. S. Kenneth, and B. G. Mette, Theory of strong-field attosecond transient absorption, J. Phys. B **49**, 062003 (2016).